

$$\begin{aligned}
 k_s(T) &= 0.133(4)\theta^{10.3(3)}, \\
 k_f(T) &= 5.68(5)\theta^{-3}10^{3.0(4)}, \\
 k_d(T) &\approx 2.2(5)\theta^{-6}10^{2.8},
 \end{aligned} \tag{8}$$

and

$$m = 0.0427/\theta^{7.3}.$$

Digits in parentheses give the standard deviation from the mean in terms of the final listed digits. Typical examples of data plots $\alpha_r(e)$ and $\alpha_r(e_1 + p)$ are exhibited in Figure 6. All experimental results supported the formulation in (5). Model predictions of the experimental data are given in Figure 14 (Section 3.4).

3. ATMOSPHERIC PROPAGATION MODEL MPM (see Appendix A and B for Details)

Dry air and atmospheric water vapor are major millimeter-wave absorbers; so are suspended droplets (haze, fog, cloud) and precipitating water drops that emanate from the vapor phase. A practical model (designated program code: MPM) was formulated that simulates the refractive index $n = n' - jn''$ of the atmospheric propagation medium for frequencies up to 1000 GHz [1] - [3]. Since the interaction with a neutral atmosphere is relatively weak, the refractive index is converted into a refractivity in units of parts per million,

$$\underline{N} = (\underline{n} - 1) 10^6 \text{ ppm.}$$

3.1 Features of the Program

A user-friendly parametric program was developed that calculates the values of the complex refractivity \underline{N} for atmospheric conditions as a function of the variables f, P, T, RH, w_A (A/B/C/D), w, and R, as listed in Appendix A (Section A.1.1).

The output of MPM are three radio path-specific quantities:

- | | | |
|--------------------|-------------|-------|
| • attenuation | $\alpha(f)$ | dB/km |
| • refractive delay | β_0 | ns/km |
| • dispersive delay | $\beta(f)$ | ps/km |

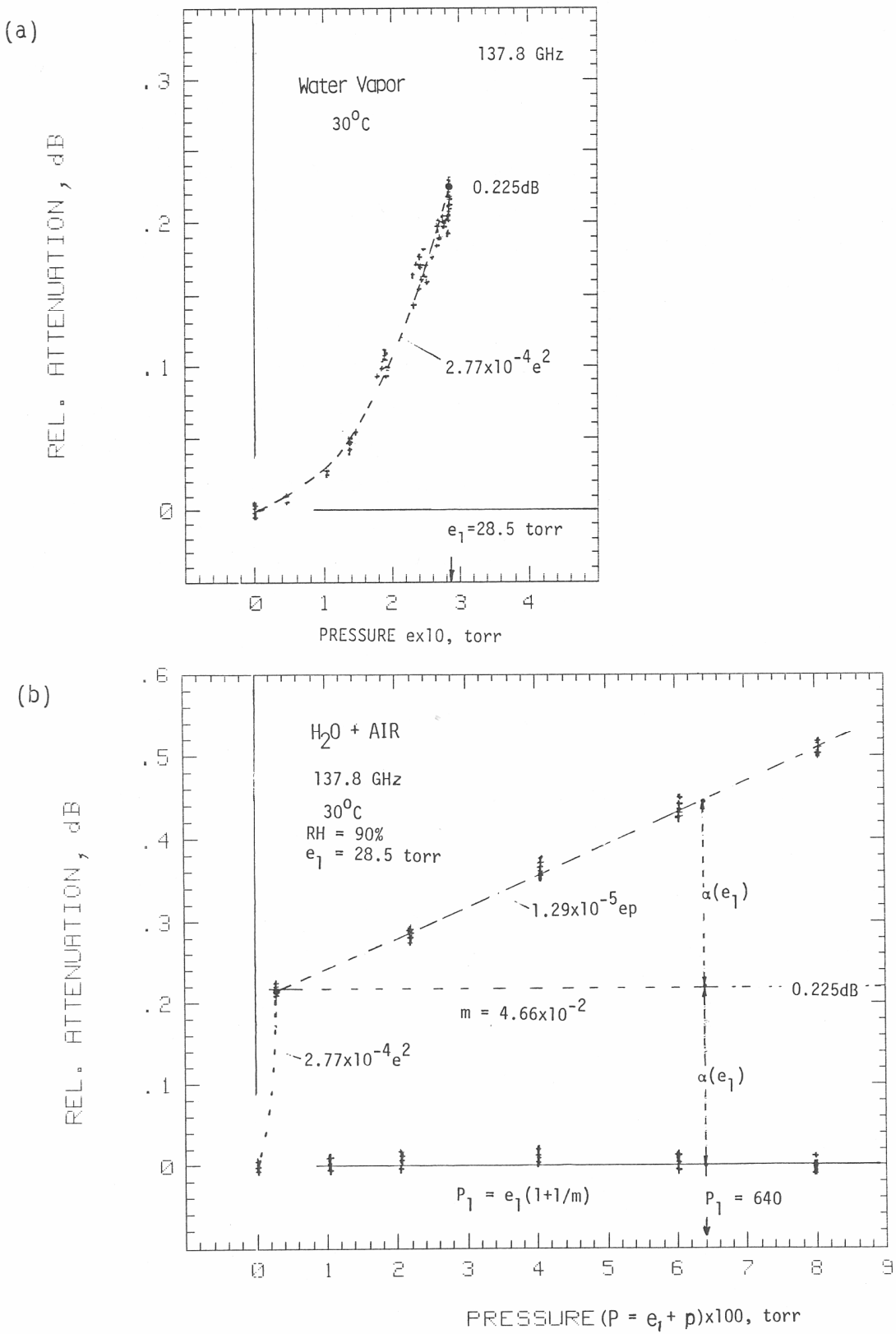


Figure 6. Typical raw data plots of relative attenuation $\alpha(P)$ for pressure scans at 137.8 GHz introducing
(a) water vapor, $P = e$, and (b) $H_2O + Air$, $P = e_1 + p$.

The height range 30 to 100 km is treated approximately excluding the detailed O₂-Zeeman effect and trace gas spectra (e.g., O₃, CO, N₂O, etc.). Program MPM is written with extensive comments to run on IBM-XT/AT + 8087 coprocessor, or equivalent, microcomputers.

Extensive revisions of the MPM code have been made recently. The latest version is described in Appendix A. Details include (a) a revised set of overlap coefficients a_5 [(A-12)] in the dry air line table (see page 66) for the 60 GHz oxygen band based on a molecular fitting scheme reported by Rosenkranz [10]; (b) a relative humidity-driven growth model for hygroscopic aerosol addressing haze conditions for RH = 90 to 99.9% [(A-3)]; (c) a new double-Debye model describing the complex permittivity $\underline{\epsilon}(f,T)$ of water for f = 0 - 1000 GHz, T = -10 to 30°C [(A-17)]; and (d) an improved fog/cloud model that includes a dispersive delay term [(A-16)].

A nonlinear least-squares fitting scheme was applied to dielectric data sets $\underline{\epsilon}(f,T)$ reported below 1 THz. Various spectral functions (relaxation and resonance) were considered, and the double-Debye model provided the best fit [15]. The Rayleigh approximation of the fog/cloud model was tested with experimental results on fog attenuation at 50, 82, 141, and 246 GHz and on differential fog delay between 246/82 GHz. All measured data were found consistent with model predictions. Moist air effects and fog effects of α and β were assumed to be additive [14].

3.2 MPM Calibration

Experimental results at 138 GHz, as described by (5) and (8), contain foremost contributions from water vapor continuum absorption. Equation (5) was used to "calibrate" the program MPM by enforcing the agreement between experimental and predicted data. The continuum, assuming an f^2 dependence, is defined by (see (14a) of [1])

$$\alpha_c = 0.1820 f N_e''(f), \quad (9)$$

where the imaginary part of refractivity N is given by (Table 3)

$$N_e'' = f(3.57 e^{2\theta} 10^{0.5} + 0.113 e p \theta^3) 10^{-5} \quad (10)$$

and f is in GHz. A comparison in Table 1 shows that at 138 GHz, within experimental uncertainties, a good fit was obtained.

In addition to (10), new width data [11] for the 183 GHz H₂O line (b_3 listed in Table 1 of [1] was increased by 11.6%) were used to update the MPM program; also, b_3 parameters of the 325 and 380 GHz H₂O lines were increased by 10 percent. Other MPM modifications were a change in the nonresonant line width γ_0 of dry air from 5.6×10^{-3} to 4.8×10^{-3} [10], the elimination of the roll-off term $1/[1 + (f/60)^2]$ (part of equation 13a in [1]), and the imposing of a high frequency cut-off $F''(f) = 0$ [see Eq. (A-9)] for $f \geq (v_0 + 40\gamma)$ [12].

3.3 Interpretation of H₂O Continuum Absorption

Since MPM employs a limited (≤ 1 THz) H₂O line base, it is of interest to find out which share of k_s and k_f (8) can be attributed to far-wing behavior of the rotational H₂O spectrum extending beyond 1 THz [6]. Results in Table 2 indicate broadening efficiency ratios ξ at 138 GHz; e.g.,

$$\xi = m(H_2O + N_2)/m(H_2O + Ar), \quad (11)$$

which are similar to those observed at cores of the 22 and 183 GHz lines. Consequently, k_f can be interpreted as a foreign-gas broadening effect whereby MPM lines account for about 30 percent of the rotational H₂O spectrum. Table 3 lists the assessment at 300 K ($\theta = 1$). When the line core argument ($m_L = 0.208/\theta^{0.5}$) is extended to k_s , then a substantial share,

Table 3. Summary Data of H_2O Line Spectrum and H_2O Excess Attenuation at 137.8 GHz, $T = 300$ K

a) Experiment-versus-MPM Predictions									
	k_s	x_s	MOIST AIR			m	x_m	DRY AIR	
			k_f	x_f				k_d	x_d
X	$\times 10^{-2}$		$\times 10^{-2}$			$\times 10^{-2}$		$\times 10^{-6}$	
M	13.2 13.15	10.5 10.51	0.570 0.5666	3.0 3.09		4.32 4.309	-7.5 -7.42	2.2 2.10	- 2.35

b) Local H_2O Lines in MPM (31% of c):						
M	0.802	3.5	0.175	3.8	21.8	0.3

c) Complete H_2O Line Spectrum ($m = 0.22$ assumed - see Table 2)						
	2.59	3.5	0.57	3.0	22	-0.5

d) Excess H_2O Absorption:						
Eq. (12)	10.3	12.5				

Table 4. Reported Data on $(\text{H}_2\text{O})_2$ Dimer Concentration e_D/e over the Temperature Range for 300 to 386 K

T , kPa	300	358.4	367.1	375.9	386.4
e , kPa	2.80	58.27	81.47	111.9	159.3
e_D , kPa	0.0024	0.44	0.76	1.28	2.27
e_D/e , $\times 10^{-3}$	0.9	7.6	9.4	11.4	14.2
e_D/e^2 , $\times 10^{-4}$	3.1	1.30	1.15	1.02	0.895
*Reference	[8]		[9]		

$$\alpha_i \simeq 0.103 e^2 \theta^{12.5} \text{ dB/km} \quad (12)$$

where $\alpha_i = (\alpha_x - \alpha_L)$ is not supported by the H₂O monomer line spectrum ($\theta^{12.5} \approx -4.3\%/\text{K}$).

At this point one might speculate about (H₂O)₂ dimer absorption. An estimate of the partial dimer vapor pressure

$$e_D \simeq 3.12 \times 10^{-4} e^2 \theta^{5} \text{ kPa}, \quad (13)$$

was obtained by fitting data on physical dimer properties given in Table 4. A strong 138 GHz attenuation rate,

$$\alpha_i \simeq 330 e_D \theta^{7.5} \text{ dB/km}, \quad (14)$$

results when (12) and (13) are combined ($\theta^{7.5} \approx -2.5\%/\text{K}$).

3.4 MPM Predictions

Features of the user-friendly atmospheric propagation model MPM were discussed in Section 3.1. The microcomputer version is written in IBM Professional FORTRAN with extensive comments that guide the user to appropriate references for specific formulations. Three parametric presentations have been found useful in practical applications, which are addressed in separate subprograms:

Profiles	Variable	Parameters
A. Frequency	f	P, T, RH(v), w _A , w, R.
B. Humidity	RH, v	f, P, T, w _A , w.
C. Pressure	P	f, T, RH(e).

A copy of the line code for program MPM-N/A (frequency profiles) is shown in Appendix B. The detailed structure of MPM comes best to light in graphical examples. Typical sea level behavior of MPM-predicted rates, α and β , is illustrated in Figures 7 to 13. Across the millimeter-wave spectrum (Figures 7 and 8) one recognizes more or less transparent window ranges (W1 to W5) separated by molecular resonance peaks. Calculations of total radio path

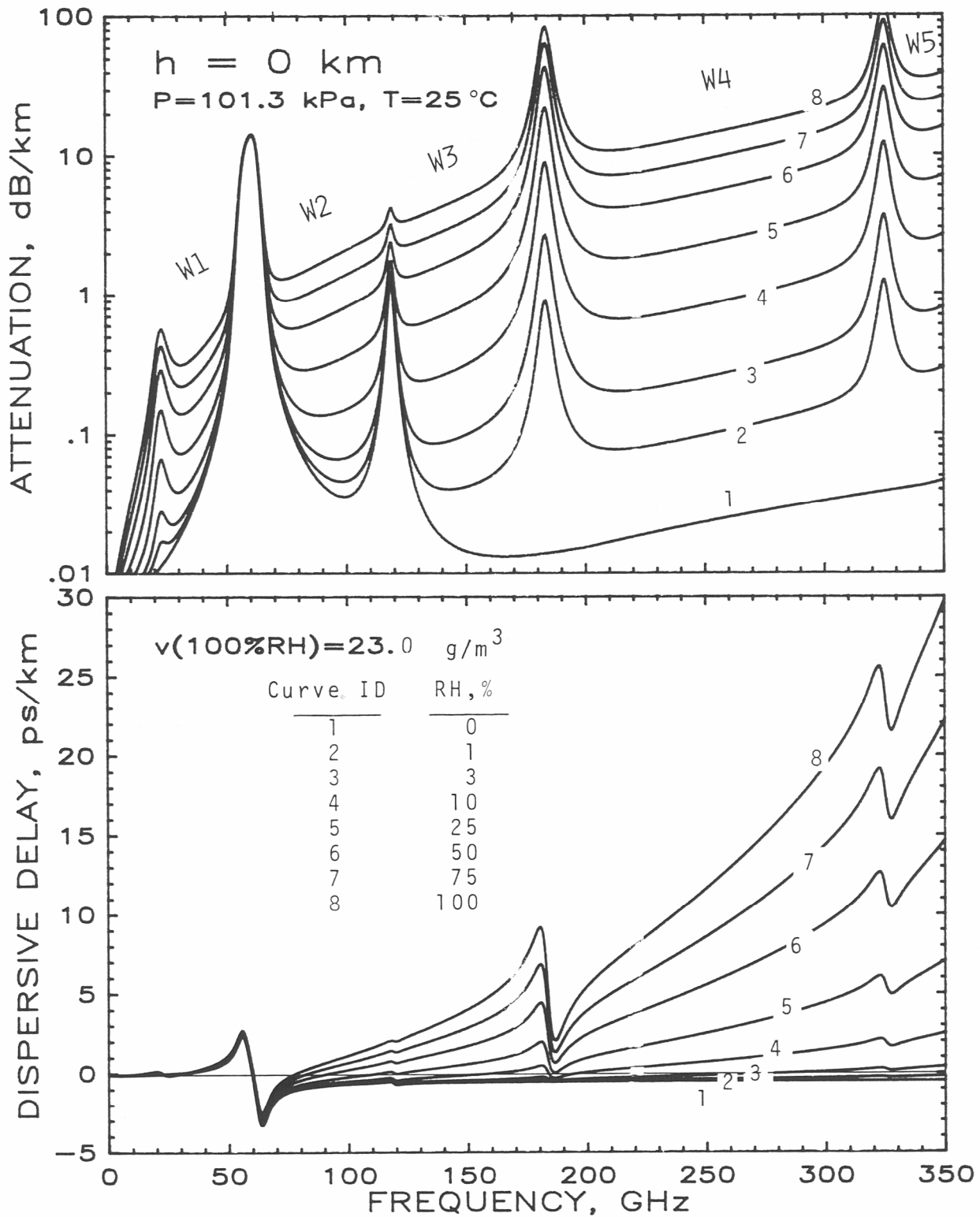


Figure 7. MPM-predicted specific values of attenuation α and dispersive delay β at sea level height $h=0 \text{ km}$ ($P=101.3 \text{ kPa}$, $T=25^\circ\text{C}$, RH=0 to 100%) over the frequency range, $f=1$ to 350 GHz. Window ranges are marked W1 to W5.

attenuation A [dB], delay B [ps], and atmospheric noise temperature T_A [K] require distributions of $P(x)$, $T(x)$, $RH(x)$ along the propagation direction x to be known [2].

Spectroscopic properties of the air-broadened water vapor line centered at 183 GHz are demonstrated in Figure 9. Accuracy of supporting line parameters (strength, width, shift) determines the reliability of predictions needed for remote sensing applications with respect to atmospheric humidity. With respect to line shape studies one observes that wing data from the delay spectrum $\beta(f)$ are unaffected by dry air pressure p . Outside a line-center frequency range $v_0 \pm 5\gamma$, dispersion $N'(f)$ is independent of a particular shape function $F'(f)$ such as (A-9b).

A major concern for most MMW systems is their performance in rain. A simplified classification of rain events is given in Appendix A (A.1.1). When neglecting any statistical nature of rain within a radio path, the calculation scheme (A-18) provides an estimate on $\alpha(f)$ and $\beta(f)$. Predictions (Figure 10) are based on adding to the known state of moist air ($P-T-RH$) only one additional parameter, namely the point rainfall rate R .

Of some importance is the fog/cloud prediction program in MPM. Systems operating in the MMW range offer an attractive alternative to electro-optical systems when operation has to be assured during periods of adverse weather (rain, cloud, fog, haze, high humidity). Current interest is focused on the frequency range 90 to 350 GHz where an optimum trade-off between atmospheric obscurations and angular resolution can be achieved. All atmospheric loss and delay effects have to be known accurately in order to analyze the potential for all-weather performance. The suspended water droplet (SWD) formulation (A-16) and (A-17) of MPM is an addition to the state of saturated air ($P-T-RH=100\%$) as illustrated in Figure 11. Key parameters are SWD content w in g/m^3 and temperature T in $^{\circ}C$.

Another atmospheric ingredient is the mass concentration w_A of hygroscopic aerosol (HAE). Solution droplets appear for $RH > 80\%$, and haze conditions develop as RH approaches 100 percent. These conditions can be modeled by assuming that at the reference humidity, $RH = 80\%$, the HAE concentration $w_A(RH = 80\%)$ is known. The RH dependent swelling/shrinking $w(RH)$ is described approximately up to $RH = 99.9\%$ by a growth model (A-3).

Relative humidity RH is the variable that governs physical processes taking place in the atmosphere with respect to water vapor. Practical models

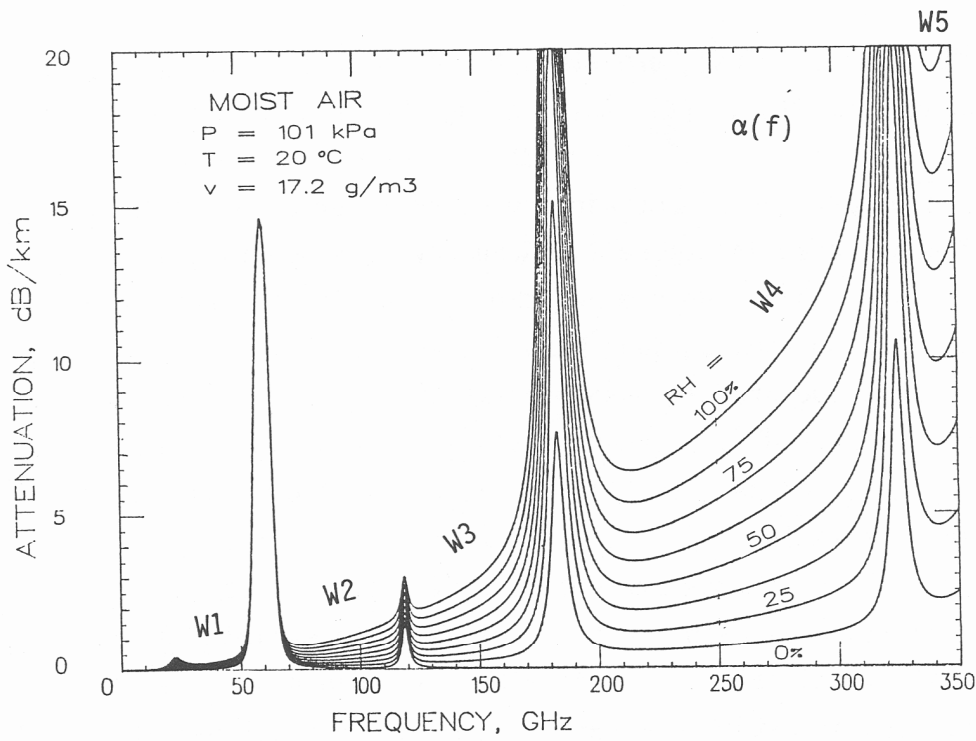


Figure 8. Water vapor absorption in window ranges for constant relative humidity increments ($\Delta RH = 12.5\%$) at a sea level condition.

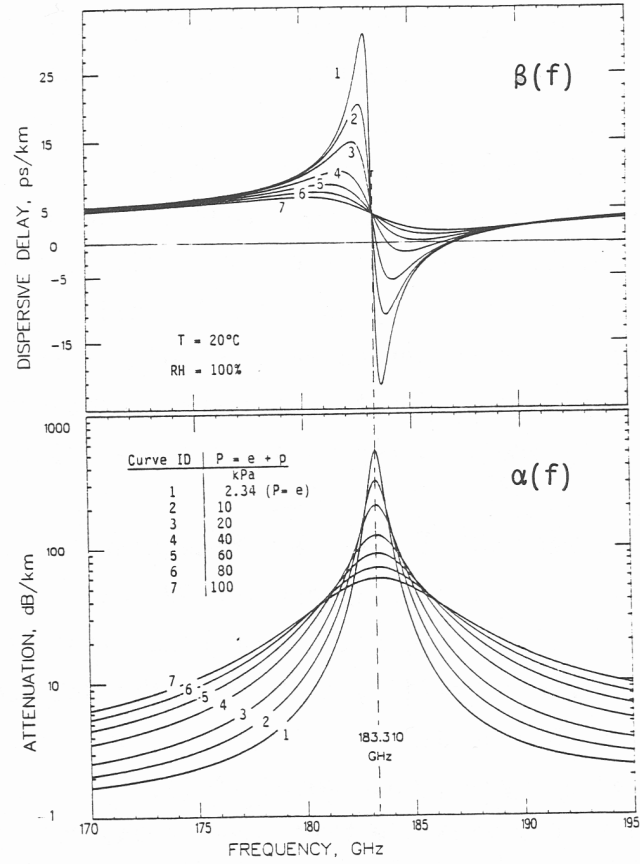


Figure 9. Pressure-broadening (AIR) example of the 183 GHz H_2O line.

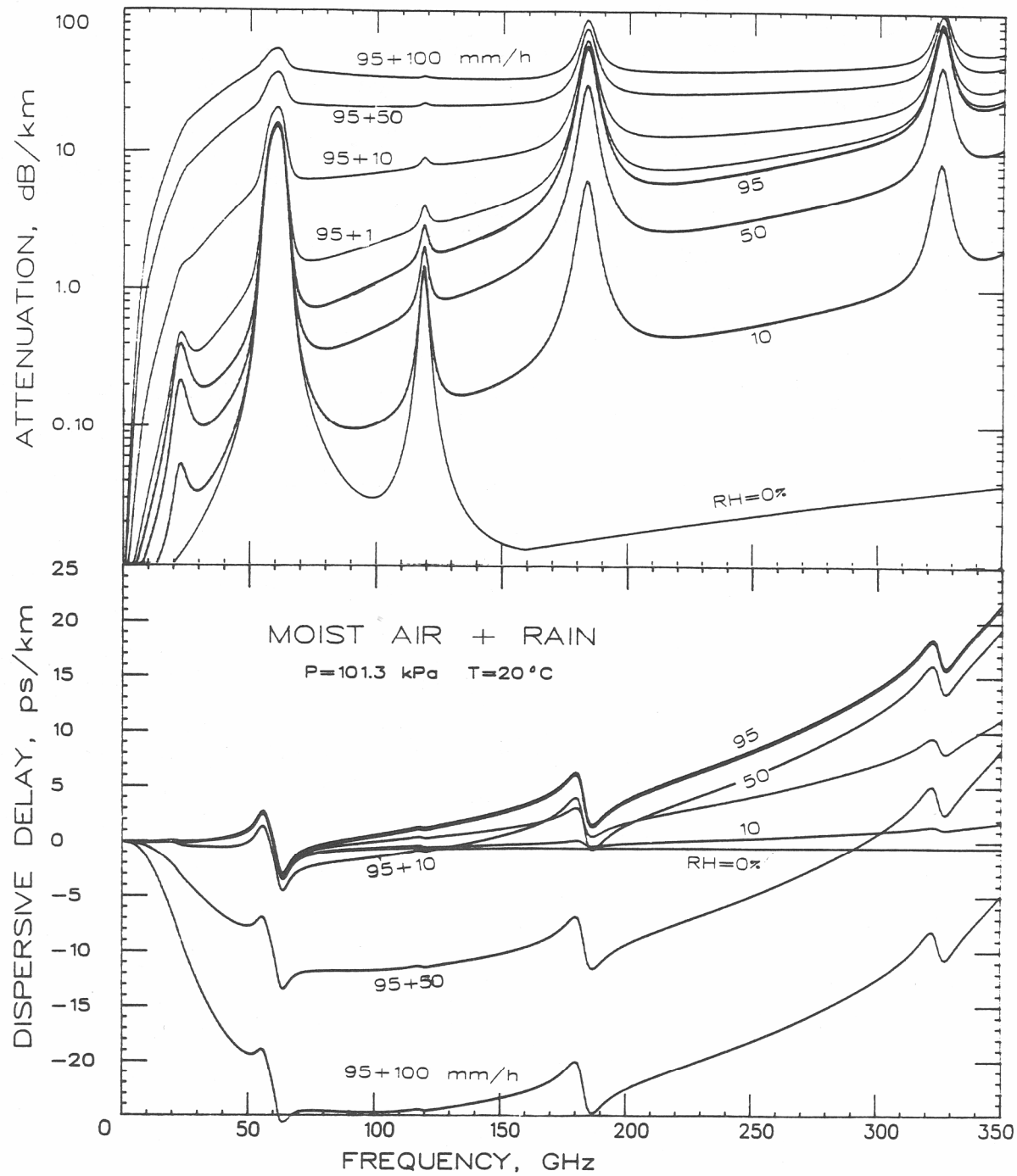


Figure 10. Attenuation α and delay β rates for three rain events ($R=10, 50,$ and 100 mm/h) added to a moist air ($\text{RH}=95\%$) sea level condition. Also shown are dry air ($\text{RH}=0\%$) and moist air ($50\% \text{ RH}$) characteristics.

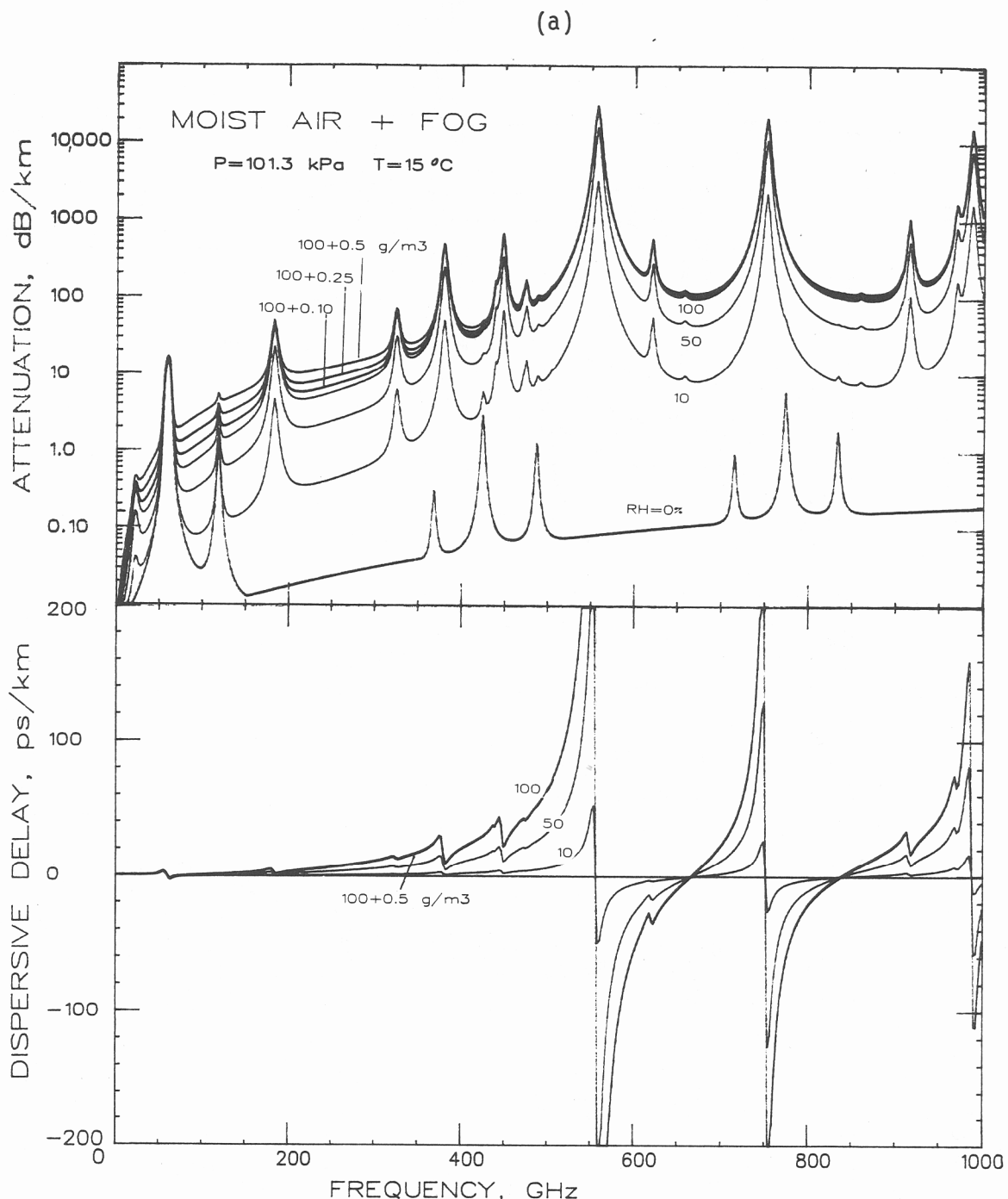


Figure 11. Attenuation α and delay β rates for three fog events ($w = 0.10, 0.25$, and 0.5 g/m^3) added to a saturated air (RH=100%) sea level condition. Also shown are dry air (0% RH) and moist air (50% RH) characteristics: (a) $f = 1\text{-}1000 \text{ GHz}$,

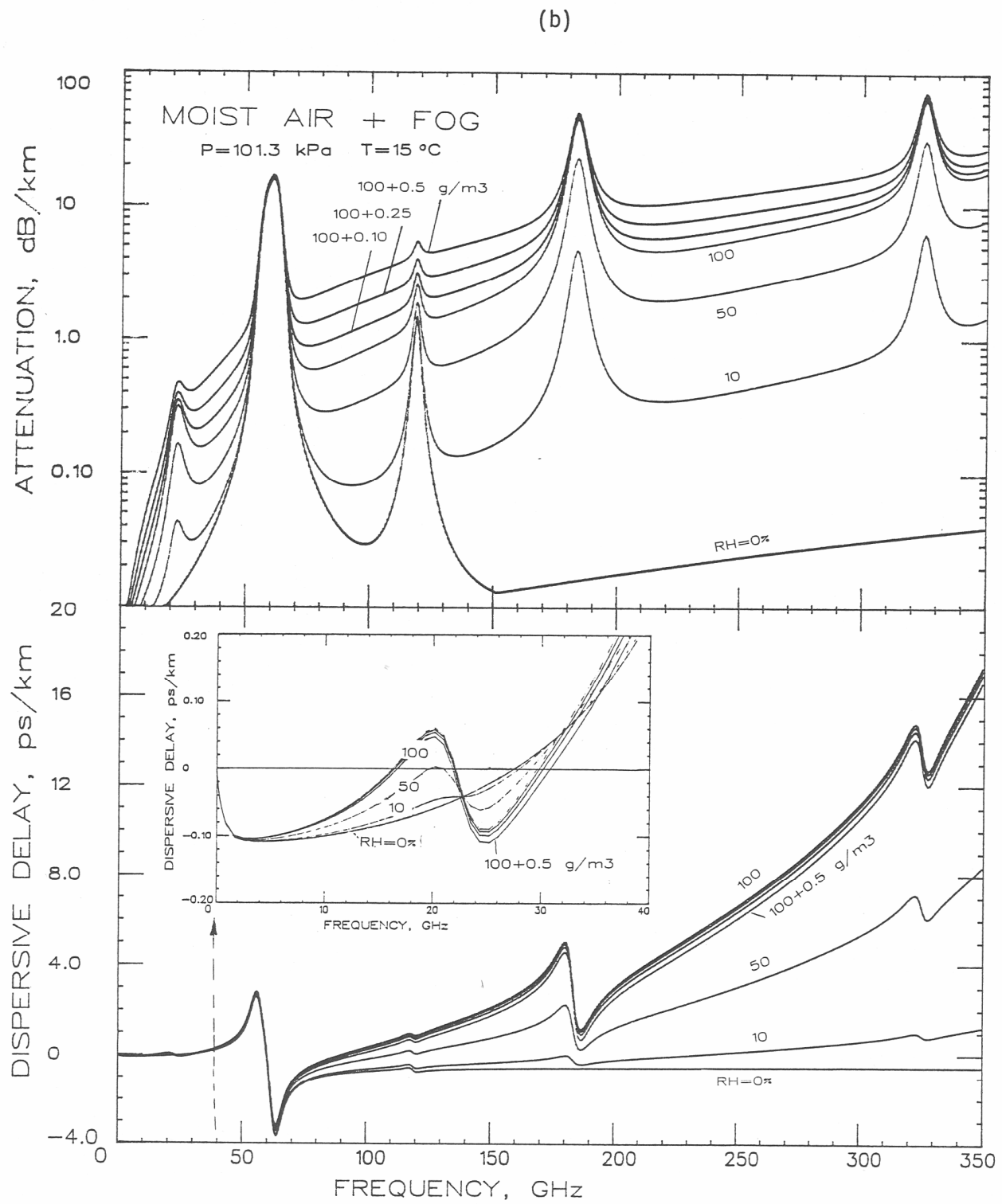


Figure 11. continued: (b) $f = 1\text{--}350$ GHz and $f = 0\text{--}40$ GHz (insert).

for RH parameterization exceeding saturation are not available. Both absolute humidity (v) and suspended haze droplet concentration (w_A) can be expressed in terms of RH variability. Absolute (v) and relative (RH) humidity are inter-related through the ambient temperature T .

Sulfates are the major RH-active ingredient of both urban and rural aerosols; so is sodium chloride for maritime species. The atmosphere is never free from HAE, with greatest concentrations near the surface and scale heights on the order of 1 km. Above RH = 90%, suspended water droplets have developed carrying the HAE essence in solutions. Average values of w_A lie between 0.01 and 1 mg/m³. The humidity parameterization in MPM is demonstrated by the examples given in Figures 12 and 13.

Pressure variability comes into play when modeling height dependencies. Cumulative calculations of α/β for a slanted radio path through the neutral atmosphere (e.g., ground-to-satellite) encounter pressures, $P = 100$ to 0 kPa, which narrows the molecular absorption lines until they vanish altogether. Pressure-, Zeeman-, and Doppler-broadening [(A-11)] have to be considered over the height range 0 to 90 km. Another need for a formulation of pressure profiles arises from spectroscopic studies applying pressure-scanning techniques. A simulation of laboratory measurements discussed in Section 2.3 is exhibited in Figure 14.

4. EXPERIMENTAL-VERSUS-MODEL (MPM) DATA

Corroborative experimental data of sufficient quality to scrutinize MPM predictions are scarce. Reliability, precision, and limited scope of supporting meteorological data often compromise the accuracy of results deduced from field observations. Generally, laboratory experiments are more accurate by simulating controlled electromagnetic and atmospheric conditions crucial to validate a specific model aspect. In this manner, contributions from water vapor lines (22 and 183 GHz) and from oxygen lines (48 to 70, 119 GHz) have been evaluated [1], [4], [10], [11], [16]. Theoretical refinements are motivated to improve the interpretation of empirical laboratory data by establishing a connection to the physics of the problem. For example, a set of our unpublished dispersion (N') results on dry air, taken during 1976 between 53.6 and 63.6 GHz, provided reference data for an elaborate reformulation of interference coefficients that describe the 60 GHz O₂ bandshape [10]. The new